

**The Molecule-Rich Tail  
of the Peculiar Galaxy NGC 2782 (Arp 215)**

Beverly J. Smith

CASA, University of Colorado, Box 389, Boulder CO 80309

Curtis Struck

Department of Physics and Astronomy, Iowa State University, Ames IA 50012

Jeffrey D. P. Kenney

Yale University Astronomy Department, New Haven CT 06520-8101

Shardha Jogee

Department of Astronomy, Caltech, Pasadena CA 91125

Received \_\_\_\_\_; accepted \_\_\_\_\_

## ABSTRACT

We present the first detection of a large quantity of molecular gas in the extended tail of an interacting galaxy. Using the NRAO 12m telescope, we have detected CO (1 – 0) at five locations in the eastern tail of the peculiar starburst galaxy NGC 2782. The CO velocities and narrow (FWHM  $\sim 50$  km s<sup>-1</sup>) line widths in these positions agree with those seen in HI, confirming that the molecular gas is indeed associated with the tail rather than the main disk. As noted previously, the gas in this tail has an apparent ‘counter-rotation’ compared to gas in the core of the galaxy, probably because the tails do not lie in the same plane as the disk. Assuming the standard Galactic conversion  $N_{H_2}/I_{CO}$  factor, these observations indicate a total molecular gas mass of  $6 \times 10^8 M_\odot$  in this tail. This may be an underestimate of the total H<sub>2</sub> mass if the gas is metal-poor. This molecular gas mass, and the implied H<sub>2</sub>/HI mass ratio of 0.6, are higher than that found in many dwarf irregular galaxies. Comparison with an available H $\alpha$  map of this galaxy, however, shows that the rate of star formation in this feature is extremely low relative to the available molecular gas, compared to  $L_{H\alpha}/M_{H_2}$  values for both spiral and irregular galaxies. Thus the timescale for depletion of the gas in this feature is very long.

*Subject headings:* Galaxies: Individual (NGC 2782) – Galaxies: ISM – Galaxies: Interactions

## 1. Introduction

Extragalactic tails and bridges are the best-known signatures of recent gravitational interactions between galaxies (e.g., Toomre & Toomre 1972). They are also often the birthsites of stars (Schweizer 1978; Mirabel et al. 1991, 1992). Understanding when and how star formation is initiated in unusual environments such as tails and bridges can provide important clues to the processes governing star formation in general, while studying the properties of gas in tails and bridges may provide information about gas behavior during galaxy interactions and collisions.

One poorly-understood factor in star formation initiation in tails and bridges is the amount and distribution of molecular gas. Because molecular gas is the material out of which stars form, it is important to measure its distribution and mass in these structures, to test theories of how star formation is triggered in tails and bridges, and to understand gas phase changes during galaxy collisions and tail/bridge formation. In an earlier NRAO 12m telescope survey of tidal tails in six interacting/merging systems, we searched for CO emission with no success (Smith & Higdon 1994). CO was also not found in the tail of the Leo Triplet galaxy NGC 3628 (Young et al. 1983), the tidal dwarf in the Arp 105 system (Duc & Mirabel 1994; Smith et al. 1998), or the HI-rich bridge of NGC 7714/5 (Struck et al. 1998). The only locations where CO has been found outside of the main disk of a galaxy is a small concentration ( $\sim 10^6 M_{\odot}$ ) of molecular gas near an extended arm in the M81 system (Brouillet et al. 1992) and a larger mass ( $10^9 M_{\odot}$ ) near the peculiar Virgo Cluster galaxy NGC 4438 (Combes et al. 1988). In the latter case, this gas is believed to have been removed from the disk by ram pressure stripping during a high velocity collision with its apparent companion, the S0 galaxy NGC 4435 (Kenney et al. 1995). In this paper, we present the first detection of a large quantity of molecular gas in an extragalactic tail, the eastern tail of the peculiar starburst galaxy NGC 2782.

## 2. NGC 2782

The peculiar galaxy NGC 2782 (Figure 1) is an isolated galaxy with two prominent tails (Smith 1991, 1994; Sandage & Bedke 1994). The longer western tail is rich in HI but faint in the optical, and the atomic gas extends well beyond the observed stars (Smith 1991; Jogee et al. 1998). The eastern tail has a gas-deficient optical knot at the tip (Smith 1994). The HI in this tail is concentrated at the base of the stellar tail (Smith 1994). HII regions are visible in this location in the Arp Atlas (1966) photograph as well as the H $\alpha$  map of Evans et al. (1996), and have been confirmed spectroscopically by Yoshida, Taniguchi, & Mirayama (1994).

Unlike most known double-tailed merger remnants (e.g., NGC 7252; Schweizer 1982), the main body of NGC 2782 has an exponential light distribution (Smith 1994; Jogee et al. 1999), indicating that its disk survived the encounter that created the tails. The HI velocities of the NGC 2782 tails (Smith 1994) are opposite those expected from the H $\alpha$  (Boer et al. 1992), HI (Smith 1994), and CO (Jogee et al. 1999) velocity fields of the galaxy core, indicating that the tails are probably in a different plane than the inner disk. The center of NGC 2782 contains a well-known nuclear starburst (Sakka et al. 1973; Balzano 1983; Kinney et al. 1984), with an energetic outflow (Boer et al. 1992; Jogee et al. 1998; Yoshida et al. 1998). The disk of NGC 2782 appears somewhat disturbed, with three prominent optical ‘ripples’ (Arp 1966; Smith 1994), one of which contains bright H II regions (Hodge & Kennicutt 1983; Smith 1994; Evans et al. 1996; Jogee et al. 1998).

The lack of an obvious companion galaxy to NGC 2782 (Smith 1991), as well as the presence of two oppositely directed tidal tails, suggests that it may be the remnant of a merger. The survival of the NGC 2782 disk, however, indicates that if it is a merger, the intruder was probably not of equal mass (Smith 1994). It is possible that the optical concentration at the end of the eastern tail is the remains of a low mass companion,

connected to the main galaxy by a stellar bridge. The presence of the ripples in the disk as well as the lack of HI at the tip of the eastern tail are consistent with the hypothesis that this companion passed through the disk of the main galaxy (Smith 1994). The striking gas/star offset in this tail may be an example of the differing behaviour of gas and stars during a galaxy collision: the gas may have been left behind as the companion passed through the larger galaxy. In the longer western tail, in contrast to the eastern tail, the HI extends beyond the optical tail (Figure 1). In the above collision scenario, the longer western tail is material torn from the main galaxy’s outer disk, which may have initially been more extended in gas than in stars.

In our previous CO survey of tidal features, we searched for CO in the longer western tail of NGC 2782 with no success (Smith & Higdon 1994). In this paper, we present new CO observations of the shorter eastern tail that reveal a large quantity of molecular gas in this feature. As noted above, this feature may be either a tail or a bridge plus companion, depending on how it formed. For convenience throughout this paper, we will simply refer to it as a tail. However, we note that it has some morphological differences from ‘classical’ tidal tails (e.g., the Antennae), in particular, the concentration of gas at the base of the stellar feature is unusual. Throughout this paper, we assume a distance of 34 Mpc ( $H_0 = 75 \text{ km s}^{-1} \text{ Mpc}^{-1}$ ) to NGC 2782.

### 3. Single Dish CO (1 – 0) Observations

NGC 2782 was observed in the CO (1 – 0) line during 1996 December, 1997 April, May, and October, and 1998 October using the 3mm SIS receiver on the NRAO 12m telescope. Two 256×2 MHz filterbanks, one for each polarization, were used for these observations, providing a total bandpass of 1300  $\text{km s}^{-1}$  centered at 2555  $\text{km s}^{-1}$  with a spectral resolution of 5.2  $\text{km s}^{-1}$ . A nutating subreflector with a beam throw of 3’ was

used, and each scan was 6 minutes long. The beamsize FWHM is  $55''$  at 115 GHz. The pointing was checked periodically with bright continuum sources and was consistent to  $10''$ . The system temperatures ranged from 300 to 400 K. Calibration was accomplished using an ambient chopper wheel.

We observed 17 positions in the NGC 2782 system. Fifteen of these were arranged in a  $5 \times 3$  grid at  $25''$  spacing. These include the center and 8 surrounding positions, as well as six positions in the eastern tidal tail. In addition, we re-observed the position in the western tidal tail previously observed by Smith & Higdon (1994) and observed another position at the tip of the western tail. In Figure 1, these positions are marked on the HI and optical maps from Smith (1994) and Jogee et al. (1998).

We have detected CO emission at 14 of the 17 observed positions in NGC 2782: the center, the surrounding positions, and five positions in the eastern tail. The sixth position in the eastern tail was not detected. The position in the western tail, previously observed but undetected by Smith & Higdon (1994), remains undetected. The position at the tip of the western tail was also undetected. The final summed scans are shown in Figures 2 – 4. Integrated fluxes, rms noise levels, peak velocities, and line widths are provided in Table 1. For the first position in the western tail, the new data have been combined with the older data. Note that the noise levels for the positions in the tails are considerably lower than for the other positions.

#### 4. Molecular Gas in the Eastern Tail of NGC 2782

The most striking result of our 12m observations is the detection of CO out in the eastern HI structure. The central velocities of the CO lines in that tail and the narrow CO line widths are consistent with those in HI (Smith 1991, 1994), showing that this molecular

gas is associated with the tail rather than the main disk. This is illustrated in Figure 5, where velocity is plotted against right ascension for both the 21 cm HI data from Smith (1994) and the new CO data. The CO and HI in the eastern tail are at a velocity of  $\sim 2620$  km s $^{-1}$ , redshifted relative to the systemic velocity of 2555 km s $^{-1}$ . The HI in the western tail is blueshifted. Both the CO and HI gas in the disk, however, are blueshifted to the east of the nucleus and redshifted to the west of the nucleus. The molecular gas in the eastern tail, like the HI, shows a reversal in velocity, an apparent ‘counter-rotation’, with respect to the gas in the inner disk. As noted previously (Smith 1994), the tails are probably not in the same plane as the disk so this may not represent a true counter-rotation in the same plane.

Converting the CO fluxes for this tail into molecular gas masses is very uncertain, because of possible metallicity and CO self-shielding effects. In tidal features, where the column densities and metallicities tend to be low, the Galactic  $I_{CO}/N_{H_2}$  ratio may underestimate the amount of molecular gas (Smith & Higdon 1994) (see Section 7). The gas in the eastern tail of NGC 2782 may be metal-poor (Yoshida et al. 1994), although this has not yet been quantified. Using the Galactic  $N_{H_2}/I_{CO}$  ratio for this tail may therefore underestimate the total amount of molecular gas present in it. For convenience in comparing with other galaxies and other tails/bridges, we will use this conversion factor ( $2.8 \times 10^{20}$  cm $^{-2}/(\text{K km s}^{-1})$ ; Bloemen et al. 1986), with the understanding that the H $_2$  mass it provides may be a lower limit to the true molecular gas mass in this feature. Possible variations to this conversion factor are discussed in detail in Section 7.

Assuming the emission fills the beam (coupling efficiency  $\eta_c = 0.82$ ), the Galactic conversion factor gives an average H $_2$  column density for the five observed locations in the eastern tail of  $2 \times 10^{20}$  cm $^{-2}$ . The CO flux does not vary wildly from position to position in this tail, showing that molecular clouds are distributed throughout the feature, not

concentrated in a single location. Integrating over all five positions in the eastern tail, the Galactic  $N_{H_2}/I_{CO}$  value gives a total molecular gas mass for this tail of  $6 \times 10^8 M_\odot$ . This is the first detection of such a large quantity of molecular gas in a tail or bridge. This mass is two orders of magnitude higher than that in the possible M81 cloud (Brouillet et al. 1992), and is similar to or greater than that found in irregular galaxies using the same conversion factor (Combes 1985; Tacconi & Young 1987).

The molecular to atomic gas mass ratio for this tail is thus 0.6. This is higher than the  $M_{H_2}/M_{HI}$  ratio derived for most dwarf irregular galaxies with the same conversion factor (Combes 1985; Tacconi & Young 1987; Israel, Tacconi, & Baas 1995). It is also higher than that found for Scd and Sm galaxies, but lower than the global values for earlier high mass spiral galaxies (Young & Knezek 1989). This ratio is consistent with the value found in the outer regions of the Milky Way and other spiral galaxies, at galactic radii of 5 – 15 kpc (Bloemen et al. 1986; Tacconi & Young 1986; Kenney, Scoville, & Wilson 1991).

## 5. Star Formation in the Eastern Tail of NGC 2782

To investigate the processes that trigger star formation in tails and bridges, it is important to quantify the star formation rates, efficiencies, and morphologies in these structures. In Figure 6, we compare the HI structure of the eastern tail with the  $H\alpha$  map from Jogee et al. (1998). This map shows at least nine H II regions in this tail (Table 2). Four of these were previously tabulated by Evans et al. (1996). Star formation is well-distributed throughout this feature, not concentrated in a single location. Calibrating the  $H\alpha$  image using the total  $H\alpha$  flux for NGC 2782 from Smith (1994) gives a total  $H\alpha$  luminosity for this tail of  $4.0 \pm 1.7 \times 10^{39} L_\odot$ . This falls within the range spanned by irregular galaxies (Hunter & Gallagher 1985; Hunter, Hawley, & Gallagher 1993), and is close to the observed  $L_{H\alpha}$  for well-known irregular galaxy NGC 6822 (Hunter et al. 1993).



Assuming an extended Miller-Scalo initial mass function (Kennicutt 1983) and no extinction correction, the total star formation rate for the eastern NGC 2782 tail is therefore between 0.01 and 0.05  $M_{\odot}$  year $^{-1}$ . The  $H\alpha$  luminosities for the observed H II regions in this tail range from  $5 \times 10^{37}$  erg s $^{-1}$  to  $3 \times 10^{38}$  erg s $^{-1}$  (Table 2), with the more luminous regions being in the south. These luminosities are similar to those of the brightest H II regions in NGC 6822 (Hodge, Lee, & Kennicutt 1989), thus these H II regions are not extremely luminous, being more than an order of magnitude fainter than the 30 Doradus H II region in the Large Magellanic Cloud (Faulkner 1967; Kennicutt 1984).

The ratio of the star formation rate to the available molecular gas for this feature,  $L_{H\alpha}/M_{H_2}$ , is 0.002  $L_{\odot}/M_{\odot}$ . This is very low, compared to global values for high mass galaxies (0.001 – 1  $L_{\odot}/M_{\odot}$ , with the majority between 0.0025 and 0.1  $L_{\odot}/M_{\odot}$ ; Young et al. 1996). This implies that the timescale for depletion of the available gas by star formation is very long, about 20 billion years. A greater-than-Galactic  $N_{H_2}/I_{CO}$  ratio in the NGC 2782 tail would make these differences even more extreme. The  $H\alpha/CO$  ratio for this tail is also low compared to irregular galaxies. For eight irregular galaxies with CO and  $H\alpha$  measurements available (from Tacconi & Young 1983; Hunter & Gallagher 1996; Hunter et al. 1993; Young et al. 1996; Madden et al. 1997; Israel 1997), the  $L_{H\alpha}/M_{H_2}$  ratios (using the Galactic conversion factor for comparison purposes) range from  $\geq 0.01$  to 1.9, much higher than our value for the NGC 2782 eastern tail. Therefore this tail has a very low star formation rate relative to its CO flux, compared to global values for galaxies in general.

## 6. Comparison With Other Tail/Bridge Features

In Table 3, we compare the HI and implied  $H_2$  column densities of the eastern NGC 2782 tail with five other extended features: the star-forming tail in the Antennae galaxy (NGC 4038/9), the NGC 7714/5 bridge, the molecular gas concentration outside of the

main disk of NGC 4438, the Magellanic Irregular in the Arp 105 system, and the northern tail of NGC 4676 (the ‘Mice’). We also include derived  $M_{H_2}/M_{HI}$  values in this table. As before, we are assuming the Galactic  $N_{H_2}/I_{CO}$  conversion factor for convenience; in Section 7, we discuss possible variations in this factor. For the star-forming Antennae tail and the Arp 105 irregular, the  $M_{H_2}/M_{HI}$  upper limits in the CO beam are  $\leq 0.2$ , much less than the detected level in the eastern NGC 2782 tail. In the bridge of the interacting pair NGC 7714/5, the CO/HI upper limit is even lower, implying  $M_{H_2}/M_{HI} \leq 0.06$ . On the other hand, in the NGC 4438 source, the CO mass is large compared to the HI mass ( $M_{H_2}/M_{HI} \sim 5$ ). Thus there is a wide range in the CO/HI ratios in these features. For NGC 4676 and the other tails measured but not detected in CO (Young et al. 1983; Smith & Higdon 1994; Duc & Mirabel 1994; Duc et al. 1997), including our new measurements of the longer western tail of NGC 2782, the HI column densities are less than that in the eastern NGC 2782 tail, and the derived  $M_{H_2}/M_{HI}$  upper limits in the CO beam are similar to or higher than the ratio for the NGC 2782 eastern tail, so we are not able to make any strong comparisons.

In Table 4, we compare the star forming properties of the eastern NGC 2782 tail with those of the other objects in Table 3. For the NGC 4438 feature, much of the ionized gas may have been ionized by shocks rather than young stars (Kenney et al. 1995). Therefore, in Table 4 we list the observed  $H\alpha$  luminosity as an upper limit to the  $H\alpha$  luminosity from young stars. Arp 105 is not included in Table 4, although star formation is on-going in the Arp 105 structure (Duc & Mirabel 1994), because no global  $H\alpha$  flux has been published for this feature to date.

The  $H\alpha$  luminosities are similar for the NGC 2782 tail, the NGC 7714/5 bridge, and the Antennae tail and a few times larger for the NGC 4676 tail. For NGC 4438, the upper limit to  $L_{H\alpha}$  is similar to the measured values for the other systems. The CO luminosity

for the eastern NGC 2782 tail and the NGC 4438 clump are much higher than in the other systems, and therefore the implied  $L_{H\alpha}/M_{H_2}$  ratios are much lower, if the  $N_{H_2}/I_{CO}$  ratios are similar. The  $L_{H\alpha}/M_{H_2}$  ratio of NGC 2782, and the upper limit for NGC 4438, are more than 7 times lower than the lower limit for the Antennae dwarf and 3 – 4 times lower than the lower limits for the NGC 7714/5 and NGC 4676 features. Thus either the rate of star formation per molecular gas mass differs from system to system, being lowest in NGC 2782 and NGC 4438, or the  $N_{H_2}/I_{CO}$  ratios are lower in NGC 2782 and NGC 4438 than in the other objects. These possibilities are discussed in Sections 7 – 9.

We also note that the spatial distributions of the H II regions vary from feature to feature for the objects in Table 4, so the average ambient ultraviolet flux differs from object to object. The nine H II regions in the NGC 2782 tail are spread out over a total area of  $60 \text{ kpc}^2$ , while in the Antennae, the three H II regions found by Mirabel et al. (1992) are located within a  $10 \text{ kpc}^2$  region. In the NGC 7714/5 bridge, the area subtended by the star forming regions is  $\sim 36 \text{ kpc}^2$ , while in the NGC 4676 tail, the H II regions in the  $55''$  ( $23 \text{ kpc}$ ) CO beam are aligned along a narrow ridge  $\sim 2 \text{ kpc}$  or less in width (Hibbard 1995; Hibbard & van Gorkom 1996). Thus the NGC 2782 H II regions are more spread out than the H III regions in these other features, therefore the ambient UV field is weaker.

The  $H\alpha$  luminosity functions also appear to differ from feature to feature. Most of the observed  $H\alpha$  in the Antennae dwarf is arising from a single luminous H II region of  $1.4 \times 10^{39} \text{ erg s}^{-1}$ ; the NGC 4676 tail contains several knots with similar luminosities (Hibbard 1995). These H II regions are more luminous than any individual H II region in the NGC 2782 feature (Table 2). In NGC 7714/5, the three brightest H II regions in the bridge (González-Delgado et al. 1995) are also more luminous than any in the NGC 2782 tail, but less luminous than the brightest in the Antennae tail.

## 7. Possible Variations in the $N_{H_2}/I_{CO}$ Ratio

In comparing the NGC 2782 tail to other features, we must first address the question of possible system-to-system differences in the  $N_{H_2}/I_{CO}$  ratio. The parameters that may affect this ratio include the metallicity and dust content, the column and volume density, and the ambient ultraviolet radiation field.

Low dust extinction, as well as low C and O abundances, leads to more CO destruction and therefore smaller CO cores in low metallicity molecular clouds (Maloney & Black 1988; Maloney 1990; Maloney & Wolfire 1996). CO interferometric studies of nearby dwarf galaxies support this scenario; the virial masses implied by the linewidths are often higher than  $H_2$  masses derived from CO fluxes using the standard Galactic conversion ratio (Dettmar & Heithausen 1989; Rubio et al. 1991, 1993a,b; Wilson 1994, 1995; Arimoto et al. 1996). There is some suggestion that the  $N_{H_2}/I_{CO}$  ratio in low metallicity systems scales with abundance, but with large scatter (Wilson 1995; Arimoto et al. 1996). One of the reasons for the observed system-to-system CO/HI variations seen in Table 3 may therefore be abundance variations. At this point, however, not enough information is available about these features to test this hypothesis. Less-than-Galactic oxygen abundances of  $12 + \log[O/H] = 8.4$  and  $8.6$  have been derived for the Antennae and Arp 105 features, respectively (Mirabel et al. 1992; Duc & Mirabel 1994). These are similar to the metallicity of the Large Magellanic Cloud (Dufour 1994; Russell & Dopita 1990), and lower than the average value for the Milky Way ( $12 + \log[O/H] = 9.0$ ; Shaver et al. 1983). For the Large Magellanic Cloud, an enhanced  $N_{H_2}/I_{CO}$  has been inferred (Cohen 1988; Israel & de Graauw 1991; Mochizuki et al. 1994; Poglitsch et al. 1995).

For the other four objects in Table 3, abundance analyses have not yet been undertaken. For the eastern tail of NGC 2782, the H II region studied by Yoshida et al. (1994) shows an enhanced  $[O III] \lambda 5007/H\beta$  ratio, hinting at a less-than-solar metallicity, however, this

has not yet been quantified. The nucleus of NGC 7714 has been shown to be metal-poor (French 1980; García-Vargas et al. 1997), but at present no abundance study has been done for the gas in the NGC 7714/5 bridge, the NGC 4438 clump, or the NGC 4676 tail. Thus it is not yet possible to determine how metallicity may be affecting the  $N_{H_2}/I_{CO}$  fluxes in these features.

CO and  $H_2$  self-shielding variations may also produce the observed CO/HI differences in these features. CO becomes self-shielding at higher column densities than  $H_2$ , leading to higher  $N_{H_2}/I_{CO}$  ratios at column densities  $N_H \leq 10^{21} \text{ cm}^{-2}$  (van Dishoeck & Black 1988; Lada et al. 1988; Blitz, Bazell, and Désert 1990). At column densities  $N_H \sim 5 \times 10^{20} \text{ cm}^{-2}$  or lower,  $H_2$  self-shielding also becomes an issue. In the local interstellar medium, the proportion of gas in molecular form decreases rapidly at a threshold level of  $\sim 5 \times 10^{20} \text{ cm}^{-2}$  (Savage et al. 1977; Federman et al. 1979). This threshold increases with decreasing density and metallicity (Elmegreen 1989).

The column densities of the features in Table 3 are in the range where the lack of CO and possibly  $H_2$  self-shielding may be important. However, the CO/HI ratio is not correlated with HI +  $H_2$  column density in this small sample. For the NGC 4438, NGC 2782, and Antennae structures, there is a trend of decreasing CO/HI ratios with decreasing HI +  $H_2$  column densities. In NGC 4438, it appears as if both the CO and  $H_2$  thresholds are exceeded, and the CO/HI ratio is very high. In the Antennae galaxy, in contrast, CO (and maybe  $H_2$ ) may not be well-shielded, and the CO/HI ratio is very low. NGC 2782 lies between these two extremes. Our detection of CO in this tail implies that the CO threshold is exceeded in at least portions of tail, but maybe not over the entire feature. NGC 7714/5 and Arp 105, however, do not fit this trend, while for NGC 4676, the CO/HI upper limit is too high to be able to make any strong constraints. Arp 105 has a similar HI column density to NGC 2782 but less CO. NGC 7714/5 has an HI column density higher than the

expected CO threshold, and higher than that of NGC 2782, and yet has a very low CO/HI upper limit. Perhaps this bridge has significantly lower abundances than the other features, and so a higher CO self-shielding threshold.

A related reason for the observed CO/HI differences in Table 3 may be variations in the clumpiness of the gas within the CO beam. In NGC 4438, the physical size of the CO beam is only 2.2 kpc,  $2.7 - 4.5 \times$  less than in the other systems, so a higher average  $H_2$  and CO column density is not surprising. In Arp 105 and NGC 4676, the beamsizes are 30 kpc and 23 kpc, respectively, so lower average CO column densities are also not unexpected. In the Antennae and NGC 7714/5 features, however, the beam subtends 6 kpc and 10 kpc, respectively, compared to 9 kpc in NGC 2782, yet the CO is much fainter. Thus there is no trend of decreasing CO/HI ratio with beamsize. Within the beam, however, there may be variations in how the gas is clumped; perhaps in the NGC 2782 feature, the CO self-shielding limit is exceeded over larger portions of the feature and so beam-dilution is less of a factor. This issue could be addressed with higher resolution CO observations.

Another important factor which affects the  $N_{H_2}/I_{CO}$  ratio is the ambient ultraviolet flux, which may be higher in the Antennae, NGC 4676, and NGC 7714/5 features than in the eastern NGC 2782 tail (see Section 6). If two systems have similar low metallicities, dust contents, and gas densities, the one with the more intense ambient ultraviolet field will have more CO destruction and so a higher average  $N_{H_2}/I_{CO}$  ratio (Maloney & Wolfire 1996). This is consistent with the difference between the CO/HI ratios of the NGC 2782 tail and the other features.

We conclude that system-to-system variations in the  $N_{H_2}/I_{CO}$  ratio likely play an important role in determining the CO/HI values of these features. However, without detailed analyses of the metal abundances in these structures we are not able to quantify these differences.

## 8. Tail/Bridge Formation Mechanisms

Another factor which may contribute to the observed variations in the CO content of tails/bridges is differences in the formation mechanisms of these structures. Two distinct processes contribute to the formation of extragalactic tails and bridges: tidal forces (e.g., Toomre & Toomre 1972) and ram pressure stripping (e.g., Spitzer & Baade 1951; Struck 1997). The relative importance of these two mechanisms probably varies from system to system: in small impact parameter collisions between gas-rich galaxies, cloud-cloud impacts and other hydrodynamical effects may be important in forming tails/bridges, while features pulled out during distant encounters may be largely tidal. Dissipation in the gas, in addition to possible pre-collision differences in the gaseous and stellar distributions, may cause large offsets between the gas and the stars in bridges and tails. Such offsets have been found in a number of systems (Wevers et al. 1984; Smith 1994; Hibbard & van Gorkom 1996; Smith et al. 1997). Gas dissipation and shocks can occur both during the initial encounter and also during subsequent passages, as tails fall back into the main galaxies (e.g., Hibbard and Mihos 1995).

The six features in Table 3 are quite different morphologically. The Antennae and Arp 105 structures are end-of-tail clumps (van der Hulst 1979; van der Hulst et al. 1994; Duc et al. 1997), while in NGC 4676 H II regions are seen along the full extent of the tail (Hibbard 1995; Hibbard & van Gorkom 1996). The NGC 2782 gas is concentrated at the base of a stellar tail, the targeted region in NGC 7714/5 is in the middle of a bridge connecting two galaxies, and the molecular concentration near NGC 4438 lies out of the plane of the galaxy. Ram pressure stripping may have played a bigger role in forming the eastern tail of NGC 2782 and the NGC 4438 clump than the other features. The NGC 2782 tail has a big gas/star offset, while in the Antennae and NGC 4676 tails, the stars and gas are coincident (van der Hulst et al. 1994; Hibbard & van Gorkom 1996). In the

Arp 105 irregular, the gas distribution is well-aligned with that of the stars, except for a slight offset at the southern end (Duc et al. 1997). The NGC 7714/5 bridge is actually two parallel bridges, one made out of stars, the other of gas, indicating that both tidal and hydrodynamical forces contributed to the formation of this feature (Smith et al. 1997). In NGC 4438, a distorted optical tail/arm lies 2 kpc away from the CO concentration (Combes et al. 1988); it is unclear whether the molecular gas is associated with this stellar structure or not (Kenney et al. 1995).

We have ordered these six features in terms of the importance of ram pressure stripping versus tidal forces in creating them. The ranking is: 1) NGC 4438, 2) NGC 2782, 3) NGC 7714/5, 4) Arp 105, the Antennae, and NGC 4676. The Antennae and NGC 4676 tails are classical tidal tails (Toomre & Toomre 1972; Barnes 1988; Mihos, Bothun, & Richstone 1993); the Arp 105 structure is also probably tidal (Duc et al. 1997). In contrast, the NGC 4438 clump is probably largely a product of ram pressure stripping (Kenney et al. 1995). The observed gas/star offsets in the NGC 2782 tail and NGC 7714/5 bridge suggest that gas dissipation played an important role in producing these features, but the existence of stellar counterparts shows that tidal forces also contributed (Smith 1994; Smith et al. 1997).

Interestingly, this splash/tidal ranking also correlates with the CO/HI ratio in these systems. The two structures with the most pronounced gas/star morphological differences have the largest CO abundances. One possible explanation for this correlation is simply a metallicity effect. In NGC 2782 and NGC 4438, where ‘splash’ probably played an important role and the impact parameters may have been smaller, the stripped gas, presumably removed from the inner disk, may be more metal-rich than material pulled from the outer disk in a grazing tidal interaction. Therefore the  $N_{H_2}/I_{CO}$  ratio may be lower than in the other systems. This possibility could be tested with detailed abundance studies.



The observed large CO fluxes from the NGC 4438 and NGC 2782 features might be considered somewhat surprising, in light of theoretical models of molecular dissociation during near head-on collisions. In fast shocks, H<sub>2</sub> and CO are dissociated (e.g., Hollenbach & McKee 1989), so in an extreme ‘splash’, where high velocity cloud-cloud collisions occur, one may expect a large proportion of the molecular gas to be dissociated (e.g., Harwit et al. 1987). Direct evidence for strong shocks is present in the optical spectrum of the NGC 4438 CO clump (Kenney et al. 1995). The existence of CO in the NGC 2782 and NGC 4438 features proves that, however they formed, the collisions/encounters were not drastic enough to dissociate all of the molecular gas, or, if the gas were indeed dissociated, sufficient time has passed for the H<sub>2</sub> to reform. The molecule formation timescale is  $\sim 10^9/n$  years/cm<sup>-3</sup> (Hollenbach & McKee 1979), so assuming the age of the NGC 2782 structure is  $\sim 2 \times 10^8$  years (Smith 1994), if the average density in this tail is  $n \geq 10$  cm<sup>-3</sup>, as expected for molecular clouds, then it is quite possible that the molecules in this feature dissociated during the collision and now have reformed.

## 9. Star Formation Initiation

One of the surprising results of this study is the low  $L_{H\alpha}/M_{H_2}$  ratio for this NGC 2782 tail. Whether or not star formation is triggered in a bridge or tail may be due in part to how much ram pressure stripping versus tidal effect occurred during the encounter. In a near-head-on encounter, one might expect more shocks and cloud fragmentation than in a more gentle tidal encounter. Theoretical models suggest that star formation may be inhibited in ‘splash’ features because of gas heating during the collision (Struck 1997), while in tidal features gravitational compression may enhance star formation (Wallin 1990). Thus in ‘splash’ features, molecular gas may be distributed in small, relatively diffuse clouds rather than concentrated in giant molecular clouds with high column densities.

These theoretical results suggest a trend in the star formation rate per molecular gas mass with increasing tidal contribution, consistent with our results: the two most likely ‘splash’ candidates have the lowest  $H\alpha/CO$  ratios in the group.

A second possibility is that the gas surface density in the NGC 2782 tail may be below a critical surface density required for gravitational collapse, as has been surmised for the outer regions of galactic disks (Kennicutt 1989). For a differentially rotating thin gas disk, the critical surface density is  $\Sigma_{crit} = \kappa\sigma_v/3.36G$  (Toomre 1964), where  $\kappa$  is the epicyclic frequency,  $\sigma_v$  is the velocity dispersion, and  $G$  is the gravitational constant. Although a tail or bridge may not be directly participating in the overall rotation of a galaxy, we apply this argument by assuming that these structures are thin, and replacing  $\kappa$  by  $2\Delta v/R$ , twice the velocity gradient southwest to northeast along the long axis of the feature (assuming the southeast to northwest shear in the tail is negligible).

In Table 4, we have included HI velocity gradients and dispersions for the other features in our sample, as well as their expected critical surface densities. For NGC 4438, the HI data from Cayette et al. (1990) are too low S/N to estimate the velocity gradient and dispersion accurately, so no critical density is derived. We note that the quoted velocity gradients are the observed gradients along the features, which do not take viewing perspective into account. Therefore the derived critical densities are quite uncertain, perhaps by a factor of a few. Within these uncertainties, the critical densities of all the features are similar, and are similar to the observed gas column densities. For the eastern NGC 2782 tail, the observed  $N_H$  is indeed lower than the predicted critical density, suggesting that the gas in this feature may be relatively stable against gravitational collapse. In fact, the observed  $N_H$  for this tail is *greater* than the expected self-shielding threshold for CO and  $H_2$ , and yet *less* than the expected critical density for gravitational collapse. This is consistent with the observation of abundant CO with relatively low  $H\alpha$  luminosity. In the NGC 7714/5

bridge, the HI column density alone is so high that it approaches the critical density for gravitational instability. The huge mass of atomic gas in this bridge alone may be enough to ignite the formation of stars and enhance the efficiency of star formation. For NGC 4676, the derived critical density is higher than the observed gas column density and for the Antennae the critical and observed densities are similar, yet these galaxies have high  $L_{H\alpha}/CO$  ratios. This comparison suggests that in the NGC 4676 tail and perhaps in the Antennae feature the beam filling factor may be low and/or the  $N_{H_2}/I_{CO}$  ratio may be higher compared to the NGC 2782 tail.

## 10. CONCLUSIONS

Using the NRAO 12m telescope, we have found evidence for  $6 \times 10^8 M_{\odot}$  of molecular gas in the eastern tail of NGC 2782. Compared to both spiral and irregular galaxies, the molecular gas content in the eastern tail of NGC 2782 is very high relative to the current rate of star formation, implying a very long timescale for gas depletion. Both the molecular gas and H II regions in this feature are very extended, spread out over a total area of  $60 \text{ kpc}^{-2}$ . Comparison with tidal or ‘splash’ regions in other galaxies shows a wide range in CO/HI and  $H\alpha/CO$  values.

We thank the telescope operators and the staff of the NRAO 12m telescope for their help in making these observations. We are pleased to acknowledge funding for this project from a NASA grant administered by the American Astronomical Society. This research has made use of the NASA/IPAC Extragalactic Database (NED) which is operated by the Jet Propulsion Laboratory under contract with NASA.

## REFERENCES

- Arimoto, N., Sofue, Y., & Tsuijimoto, T. 1996, PASJ, 48, 275
- Arp, H. C. 1966, Atlas of Peculiar Galaxies (Pasadena: California Institute of Technology)
- Balzano, V. A. 1983, ApJ, 268, 602
- Barnes, J. E. 1988, ApJ, 331, 699
- Blitz, L., Bazell, D., & Désert, F. X. 1990, ApJ, 352, L13
- Bloemen, J. B. G. M., et al. 1986, A&A, 154, 25
- Boer, B., Schultz, H. & Keel, W. C. 1992, A&A, 154, 25
- Brouillet, N., Henkel, C., & Baudry, A. 1992, A&A, 262, L5
- Cayatte, V., van Gorkom, J. H., Balkowski, C., & Kotanyi, C. 1990, AJ, 100, 604
- Cohen, R. S., Dame, T. M., Garay, G., Montani, Rubio, M., & Thaddeus, P. 1988, ApJ, 331, L95
- Combes, F. 1985, Star Forming Dwarf Galaxies and Related Objects, edited by D. Kunth, T. X. Thuan, and J. Tran Thanh Van (Kim Hup Lee, Singapore), 307
- Combes, F., Dupraz, C., Casoli, F., & Pagani, L. 1988, A&A, 203, L9
- Dettmar, R.-J., & Heithansen, A. 1989, ApJ, 344, L61
- Duc, P.-A., Brinks, E., Wink, J. E., & Mirabel, I. F. 1997, A&A, 326, 537
- Duc, P.-A., & Mirabel, I. F. 1994, A&A, 289, 83.
- Dufour, R. J. 1984, in IAU Symposium 108, Structure and Evolution of the Magellanic Clouds, ed. S. van den Bergh and K. S. de Boer (Dordrecht: Reidel), p. 353
- Elmegreen, B. G. 1989, ApJ, 338, 178
- Elmegreen, D. M., Kaufman, M., Brinks, E., Elmegreen, B. G., & Sundin, M. 1995, ApJ, 453, 100

- Evans, I. N., Koratkar, A. P., Storchi-Bergmann, T., Kirkpatrick, H., Heckman, T. M., & Wilson, S. A. 1996, *ApJS*, 185, 93
- Faulkner, D. J. 1967, *MNRAS*, 135, 401
- Federman, S. R., Glassgold, A. E., & Kwan, J. 1979, *ApJ*, 227, 466
- Freedman, W. L., et al. 1994, *ApJ*, 435, L31
- French, H. B. 1980, *ApJ*, 240, 41
- García-Vargas, M. L., González-Delgado, R. M., Pérez, E., Alloin, D., Díaz, A., & Terlevich, E. 1997, *ApJ*, 478, 112
- González-Delgado, R. M., Pérez, E., Díaz, A. I., García-Vargas, M. L., Terlevich, E., & Vilchez, J. M. 1995, *ApJ*, 439, 604
- Harwit, M., Houck, J. R., Soifer, B. T., & Palumbo, G. G. C. 1987, *ApJ*, 315, 28
- Hibbard, J. E. 1995, Ph. D. Thesis, Columbia University
- Hibbard, J. E., & Mihos, J. C. 1995, *AJ*, 110, 140
- Hibbard, J. E., & van Gorkom, J. H. 1996, *AJ*, 111, 655.
- Hodge, P. W., Lee, M. G., & Kennicutt, R. C., Jr. 1989, *PASP*, 101, 32
- Hodge, P. W., & Kennicutt, R. C. 1983, *AJ*, 88, 296
- Hollenbach, D., & McKee, C. F. 1989, *ApJ*, 342, 306
- Hunter, D. A., & Gallagher, J. S. 1985, *ApJS*, 58, 533
- Hunter, D. A., Hawley, W. N., & Gallagher, J. S. 1993, *AJ*, 106, 1797
- Irwin, J. A. 1994, *ApJ*, 429, 618
- Israel, F. P., & de Graauw, Th. 1991, in *IAU Symposium 148, The Magellanic Clouds*, ed. R. Haynes and D. Milne (Boston: Kluwer), p. 45
- Israel, F. P., Tacconi, L. J., & Baas, F. 1995, *A&A*, 295, 599

- Israel, F. P. 1997, *A&A*, 317, 65
- Jacoby, G. H., et al. 1992, *PASP*, 104, 599
- Jogee, S., Kenney, J. D. P., & Smith, B. J. 1998, *ApJ*, 494, L185
- Jogee, S., Kenney, J. D. P., & Smith, B. J. 1999, *ApJ*, in preparation
- Kaufman, M., Brinks, E., Elmegreen, D. M., Thomasson, M., Elmegreen, B. G., Struck, C., & Klaric, M. 1997, *AJ*, 114, 2323
- Kenney, J. D. P., Rubin, V. C., Planesas, P., & Young, J. S. 1995, *ApJ*, 438, 135
- Kenney, J. D. P., Scoville, N. Z., & Wilson, C. D. 1991, *ApJ*, 366, 432
- Kennicutt, R. C. 1983, *ApJ*, 272, 54
- Kennicutt, R. C. 1984, *ApJ*, 287, 116
- Kennicutt, R. C. 1989, *ApJ*, 344, 685
- Lada, C. L., Margulis, M., Sofue, Y., Nakai, N., & Handa, T. 1988, *ApJ*, 328, 143
- Madden, S. C., Poglitsch, A., Geis, N., Stacey, G. J., & Townes, C. H. 1997, *ApJ*, 483, 200
- Maloney, P. 1990, in *The Interstellar Medium in Galaxies*, edited by H. Thronson and M. Shull (Kluwer Academic Press, Boston), p. 493
- Maloney, P., & Wolfire, M. G. 1996, *IAU Symposium 170, CO: Twenty-Five Years of Millimeter-Wave Spectroscopy* (Tucson, AZ)
- Maloney, P., & Black, J. H. 1988, *ApJ*, 325, 389
- Mihos, J. C., Bothun, G. D., & Richstone, D. O. 1993, *AJ*, 418, 82
- Mirabel, I. F. et al. 1991, *A&A*, 243, 367
- Mirabel, I. F. et al. 1992, *A&A*, 256, L19
- Mochizuki, K. et al. 1994, *ApJ*, 430, L37

- Morris, S. L., & van den Bergh, S. 1994, *ApJ*, 427, 696
- Poglitsch, A., Krabbe, A., Madden, S. C., Nikola, T., Geis, N., Johansson, L. E. B., Stacey, G. J., & Sternberg, A. 1995, *ApJ*, 454, 293
- Rubio, M., Garay, G., Montani, J., & Thaddeus, P. 1991, *ApJ*, 368, 173
- Rubio, M., et al. 1993a, *A&A*, 271, 1
- Rubio, M., Lequeux, J., & Boulanger, F. 1993b, *A&A*, 271, 9
- Russell, S. C., & Dopita, M. A. 1990, *ApJS*, 74, 93
- Sakka, K., Oka, S., & Wakamatsu, K. 1973, *PASJ*, 25, 153
- Sandage, A., & Bedke, J. 1994, *The Carnegie Atlas of Galaxies* (Washington D.C.: Carnegie Institute)
- Savage, B. D., Drake, J. F., Budich, W., & Bohlin, R. C. 1977, *ApJ*, 216, 291
- Schweizer, F. in *Structure and Properties of Nearby Galaxies*, 1978, 279.
- Schweizer, F. 1982, *ApJ*, 252, 455
- Shaver, P. A., McGee, R. X., Newton, L. M., Danks, A. C., & Pottash, 1983, *MNRAS*, 204, 53
- Smith, B. J. 1991, *ApJ*, 378, 39
- Smith, B. J. 1994, *AJ*, 107, 1695
- Smith, B. J. 1997, *AJ*, 114, 2177
- Smith, B. J., & Higdon, J. L. 1994, *AJ*, 108, 837
- Smith, B. J., Struck, C., & Pogge, R. W. 1997, *ApJ*, 483, 754
- Smith, B. J., et al. 1998, in preparation
- Spitzer, L, Jr., & Baade, W. 1951, *ApJ*, 113, 413

- Struck, C. 1997, *ApJS*, 113, 269
- Struck, C. et al. 1998, in preparation.
- Tacconi, L. J., & Young, J. S. 1986, *ApJ*, 308, 600
- Tacconi, L. J., & Young, J. S. 1987, *ApJ*, 322, 681
- Toomre, A. 1964, *ApJ*, 139, 1217
- Toomre, A., & Toomre, J. 1972, *ApJ*, 178, 623
- van der Hulst, J. M. 1979, *AJ*, 71, 131
- van der Hulst, J. M., Mahoney, J. H., & Burke, B. F. 1994, preprint
- van Dishoeck, E. F., & Black, J. H. 1988, *ApJ*, 334, 771
- Wallin, J. F. 1990, *AJ*, 100, 1477
- Wilson, C. D. 1994, *ApJ*, 434, L11
- Wilson, C. D. 1995, *ApJ*, 448, L97
- Wevers, B. M. H. R., Appleton, P. N., Davies, R. D., & Hart, L. 1984, *A&A*, 140, 125
- Young, J. S., Allen, L., Kenney, J. D. P., Lesser, A., & Rownd, B. 1996, *AJ*, 112, 1903
- Young, J. S., & Knezek, P. M. 1989, *ApJ*, 366, L11
- Young, J. S., Tacconi, L. J., & Scoville, N. Z. 1983, *ApJ*, 269, 136
- Yoshida, M., Taniguchi, Y., & Murayama, T. 1994, *PASJ*, 46, L195
- Yoshida, M., Taniguchi, Y., & Murayama, T. 1998, *AJ*, submitted

### **Captions**

Fig. 1.— The 21 cm HI map of NGC 2782 (greyscale; from Smith 1994), overlaid on the optical B band image (contours; from Jogee et al. 1998). The optical map has been smoothed



**Table 1**

CO (1-0) RESULTS FOR NGC 2782

Name	Position Observed						$T_{R}^*$ (rms) (mK)	$I_{CO}^a$ (K km s <sup>-1</sup> )	$V_{peak}$ (km s <sup>-1</sup> )	$\Delta V^b$ (km s <sup>-1</sup> )
	R.A. (1950)	Dec. (1950)								
Center	9 10	53.6 40 19	15.0	5.1	$5.98 \pm 0.22$	2560	360			
North	9 10	53.6 40 19	40.0	7.3	$3.36 \pm 0.33$	2550	400			
South	9 10	53.6 40 18	50.0	6.0	$4.37 \pm 0.28$	2550	620			
East	9 10	55.8 40 19	15.0	6.6	$2.21 \pm 0.31$	2540	420			
West	9 10	51.4 40 19	15.0	6.8	$3.37 \pm 0.32$	2590	420			
Northwest	9 10	51.4 40 19	40.0	5.1	$3.00 \pm 0.27$	2570	520			
Northeast	9 10	55.8 40 19	40.0	6.4	$1.87 \pm 0.28$	2550	360			
Southeast	9 10	55.8 40 18	50.0	6.7	$2.57 \pm 0.31$	2480	420			
Southwest	9 10	51.4 40 18	50.0	5.0	$1.60 \pm 0.24$	2640	440			
North-Far-East	9 10	58.0 40 19	40.0	3.1	$0.73 \pm 0.09$	2600	180			
Far-East	9 10	58.0 40 19	15.0	2.6	$0.31 \pm 0.06$	2620	90			
South-Far-East	9 10	58.0 40 18	50.0	2.3	$0.44 \pm 0.05$	2630	90			
North-Far-Far-East	9 11	0.2 40 19	40.0	2.5	$\leq 0.18$		110 <sup>d</sup>			
Far-Far-East	9 11	0.2 40 19	15.0	3.1	$0.39 \pm 0.07$	2620	105			
South-Far-Far-East	9 11	0.2 40 18	50.0	3.5	$0.57 \pm 0.08$	2620	110			
Western Tail I	9 10	41.1 40 20	16.0	3.6 <sup>c</sup>	$\leq 0.22^d$		80 <sup>d</sup>			
Western Tail II	9 10	36.1 40 22	22.0	3.1	$\leq 0.19^d$		80 <sup>d</sup>			

<sup>a</sup> $I_{CO} = \int T_{R}^* dv$ .

<sup>b</sup>Full width zero maximum (FWZM).

<sup>c</sup>Combined with the Smith & Higdon (1994) data.

<sup>d</sup>Using the HI FWZM line width (Smith 1991).

to  $3''$  resolution; the HI map, to  $12''$ . The 17 positions observed in the CO (1 – 0) line with the NRAO 12m telescope are marked as crosses.

Fig. 2.— The CO spectra for the nine positions in the main disk of NGC 2782: the center and the surrounding eight positions. For displaying purposes, these spectra have been smoothed by a  $36 \text{ km s}^{-1}$  boxcar and then resampled at  $21 \text{ km s}^{-1}$  spacing.

Fig. 3.— The CO spectra for the six positions in the eastern tail of NGC 2782. These data have been smoothed and resampled as in Figure 2.

Fig. 4.— The CO spectra for the observed positions in the western tail. These data have been smoothed and resampled as in Figure 2. Position I is the more southern position in the western tail.

Fig. 5.— A right ascension-velocity map for NGC 2782. The contours and greyscale are the 21 cm HI data from Smith (1994). The crosses mark the central velocities of the 12m CO lines. The HI data have been averaged over declination. The redshifted structure at  $9^{\text{h}} 10^{\text{m}} 58^{\text{s}}$  is the eastern tail; the blueshifted feature at  $9^{\text{h}} 10^{\text{m}} 40^{\text{s}}$  is the western tail. The disk lies at  $9^{\text{h}} 10^{\text{m}} 53^{\text{s}}$ , and is blueshifted to the east and redshifted to the west.

Fig. 6.— The 21 cm HI map of NGC 2782 (greyscale; from Smith 1994), overlaid with  $\text{H}\alpha$  contours (from Jogee et al. 1998). The  $\text{H}\alpha$  map has been smoothed by a  $1''$  Gaussian to emphasize the faint H II regions. The first contour level corresponds to  $\log F_{\text{H}\alpha} = -16.5$ , where  $F_{\text{H}\alpha}$  is in units of  $\text{erg s}^{-1} \text{ cm}^{-2} \text{ arcsec}^{-2}$ . The contour interval is  $\log F_{\text{H}\alpha} = 0.2$ . The crosses mark the locations of our CO beams. The feature at  $9^{\text{h}} 10^{\text{m}} 58^{\text{s}}$ ,  $40^{\circ} 19' 8''$  is likely an artifact from imperfect stellar subtraction.

**Table 2**

The H II Regions in the Eastern NGC 2782 Tail

H II	R.A. (1950)			Dec. (1950)			$L_{H\alpha}$
Region	h	m	s	°	'	"	( $\text{erg s}^{-1}$ )
A	9	10	59.8	40	18	40.3	$3.3 \times 10^{38}$
B	9	10	58.9	40	18	46.3	$3.1 \times 10^{38}$
C	9	10	60.0	40	19	2.7	$1.2 \times 10^{38}$
D	9	11	0.7	40	19	10.7	$6.3 \times 10^{37}$
E	9	10	58.7	40	19	14.2	$2.2 \times 10^{38}$
F	9	11	1.0	40	19	21.0	$1.0 \times 10^{38}$
G	9	10	58.3	40	19	21.6	$5.7 \times 10^{37}$
H	9	10	59.5	40	19	23.9	$9.7 \times 10^{37}$
I	9	10	58.8	40	19	46.1	$4.7 \times 10^{37}$

**Table 3**

Gas Properties of Selected Tail/Bridge Features<sup>a</sup>

Feature	$N_{HI}$ ( $\text{cm}^{-2}$ )	$N_{H_2}^b$ ( $\text{cm}^{-2}$ )	$N_H^b$ ( $\text{cm}^{-2}$ )	$M_{H_2}/M_{HI}^b$	Notes
NGC 2782 Eastern Tail	$6 \times 10^{20}$	$2 \times 10^{20}$	$10^{21}$	0.6	<sup>c</sup>
Antennae Tail	$4 \times 10^{20}$	$\leq 4.2 \times 10^{19}$	$4.0 - 4.8 \times 10^{20}$	$\leq 0.2$	<sup>d</sup>
NGC 7714/5 Bridge	$1.6 \times 10^{21}$	$\leq 5.0 \times 10^{19}$	$1.6 - 1.7 \times 10^{21}$	$\leq 0.06$	<sup>e</sup>
NGC 4438 CO Clump	$9.2 \times 10^{20}$	$2.0 \times 10^{21}$	$4.9 \times 10^{21}$	5	<sup>f</sup>
Arp 105 Irregular	$7 \times 10^{20}$	$\leq 8.0 \times 10^{19}$	$7 - 9 \times 10^{20}$	$\leq 0.2$	<sup>g</sup>
NGC 4676 Northern Tail	$2.1 \times 10^{20}$	$\leq 5.9 \times 10^{19}$	$2.1 - 3.2 \times 10^{20}$	$\leq 0.6$	<sup>h</sup>

<sup>a</sup>All values are averaged over the 55'' 12m beam, except for NGC 4438, where a 23'' beam was used.

<sup>b</sup>The  $H_2$  column density and mass were derived using the Galactic  $N_{H_2}/I_{CO}$  ratio of  $2.8 \times 10^{20} \text{ cm}^{-2}/(\text{K km s}^{-1})$  (Bloemen et al. 1986), assuming the source fills the beam with a coupling efficiency of  $\eta_c = 0.82$ . Although this conversion factor may not hold in these features (see text), we use it for comparative purposes here.

<sup>c</sup> $N_{HI}$  for the NGC 2782 tail was obtained from the Smith (1994) HI map.

<sup>d</sup> $N_{HI}$  for the Antennae dwarf is from van der Hulst et al. (1994), as given in Smith & Higdon (1994). The CO flux for the Antennae dwarf is from Smith & Higdon (1994).

<sup>e</sup>The HI column density for the NGC 7714/5 bridge is from the Smith et al. (1997) HI data. The CO flux is from Struck et al. (1998).

<sup>f</sup>For the NGC 4438 molecular concentration,  $N_{HI}$  is from Cayatte et al. (1990) and the CO flux is from Combes et al. (1988).

<sup>g</sup>For Arp 105, the HI column density is from Duc et al. (1997) and the CO upper limit is from Smith et al. (1998), with the HI FWZM line width of  $220 \text{ km s}^{-1}$  from Duc et al. (1997).

<sup>h</sup>For NGC 4676, the CO flux is from Smith & Higdon (1994) and the HI flux is from Hibbard (1995), as quoted in Smith & Higdon (1994).

**Table 4**

Star Forming Properties of Selected Tail/Bridge Features<sup>a</sup>

Galaxy	D <sup>b</sup> (Mpc)	L <sub>H<math>\alpha</math></sub> (erg s <sup>-1</sup> )	M <sub>H<sub>2</sub></sub> <sup>c</sup> (M <sub><math>\odot</math></sub> )	L <sub>H<math>\alpha</math></sub> /M <sub>H<sub>2</sub></sub> (L <sub><math>\odot</math></sub> /M <sub><math>\odot</math></sub> )	$\Delta v/R$ (km s <sup>-1</sup> kpc <sup>-1</sup> )	$\sigma_v$ (km s <sup>-1</sup> )	N <sub>crit</sub> (cm <sup>-2</sup> )	Notes
NGC 2782	34	$4 \times 10^{39}$	$6 \times 10^8$	0.002	5.1	20	$2 \times 10^{21}$	<i>d</i>
Antennae	23	$1.7 \times 10^{39}$	$\leq 2.9 \times 10^7$	$\geq 0.015$	2.2	10	$4 \times 10^{20}$	<i>e</i>
NGC 7714/5	37	$1.8 \times 10^{39}$	$\leq 9.4 \times 10^7$	$\geq 0.005$	3.5	10	$6 \times 10^{20}$	<i>f</i>
NGC 4438	16	$\leq 1.6 \times 10^{39}$	$8.4 \times 10^8$	$\leq 0.0005$				<i>g</i>
NGC 4676	88	$1.1 \times 10^{40}$	$\leq 6.0 \times 10^8$	$\geq 0.01$	5.5	10	$9 \times 10^{20}$	<i>h</i>

<sup>a</sup>For the Antennae, NGC 7714/5, and NGC 4676, the tabulated values are averaged over the 55" NRAO 12m beam. For NGC 2782 and 4438, values for the entire tail are used.

<sup>b</sup>Assuming  $H_0 = 75 \text{ km s}^{-1} \text{ Mpc}^{-1}$ , except for the Virgo Cluster galaxy NGC 4438, where 16 Mpc is used (Jacoby et al. 1992; Freedman et al. 1994).

<sup>c</sup>The H<sub>2</sub> masses were derived using the Galactic N<sub>H<sub>2</sub></sub>/I<sub>CO</sub> ratio (Bloemen et al. 1986; see discussion in text), assuming  $\eta_c = 0.82$ .

<sup>d</sup>For NGC 2782,  $\Delta v/R$  and  $\sigma_v$  were obtained from the Smith (1994) HI map. The velocity dispersions in this feature range from 15 – 30 km s<sup>-1</sup> at the base of the tail to 10 – 20 km s<sup>-1</sup> in the rest of the feature.

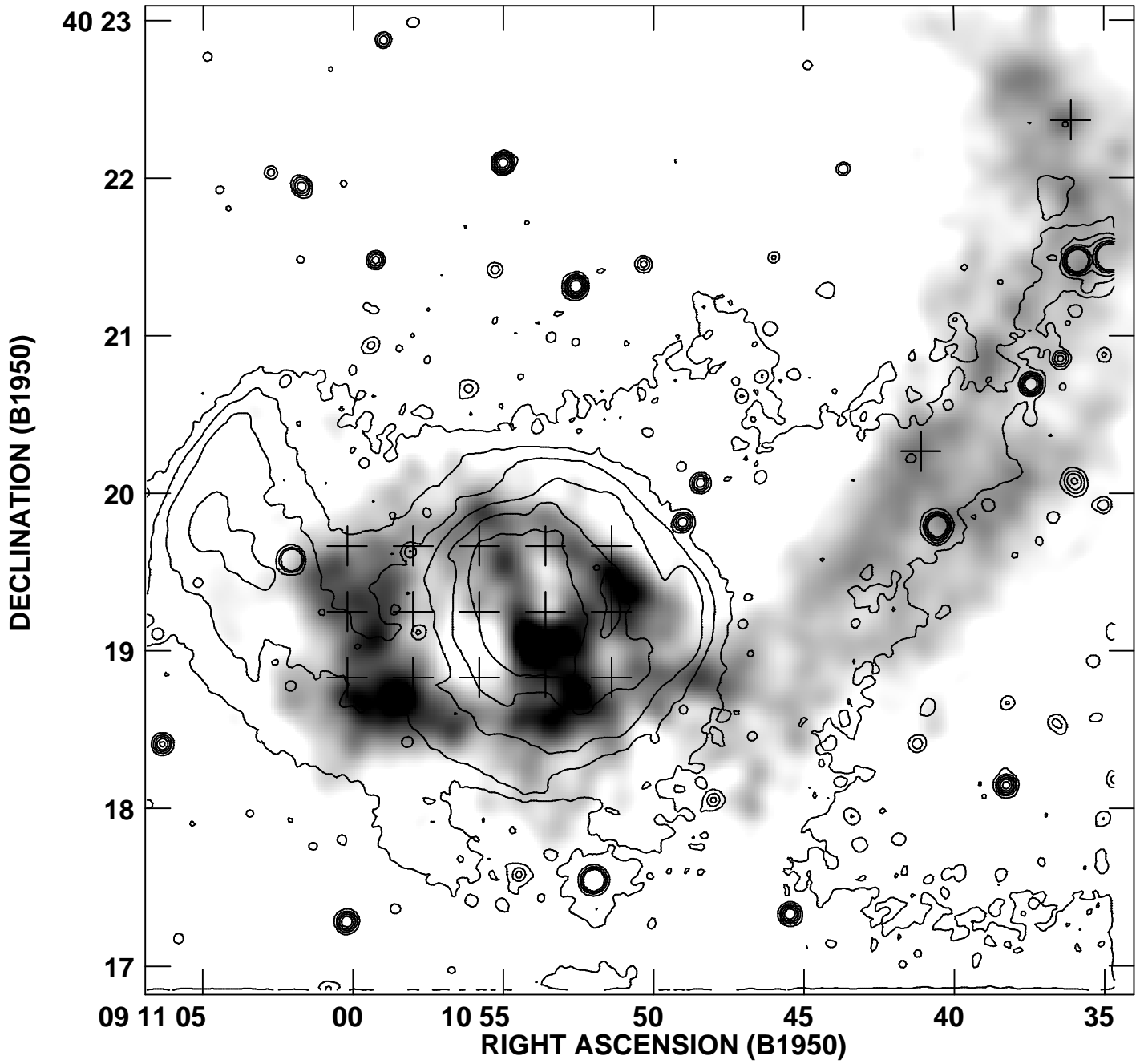
<sup>e</sup>For the Antennae,  $\Delta v/R$  and  $\sigma_v$  are from Hibbard (1998, private communication). L<sub>H $\alpha$</sub>  is from Mirabel et al. (1992).

<sup>f</sup>For the NGC 7714/5 bridge,  $\Delta v/R$  and  $\sigma_v$  were obtained from the Smith et al. (1997) HI data. L<sub>H $\alpha$</sub>  is from González-Delgado et al. (1995).

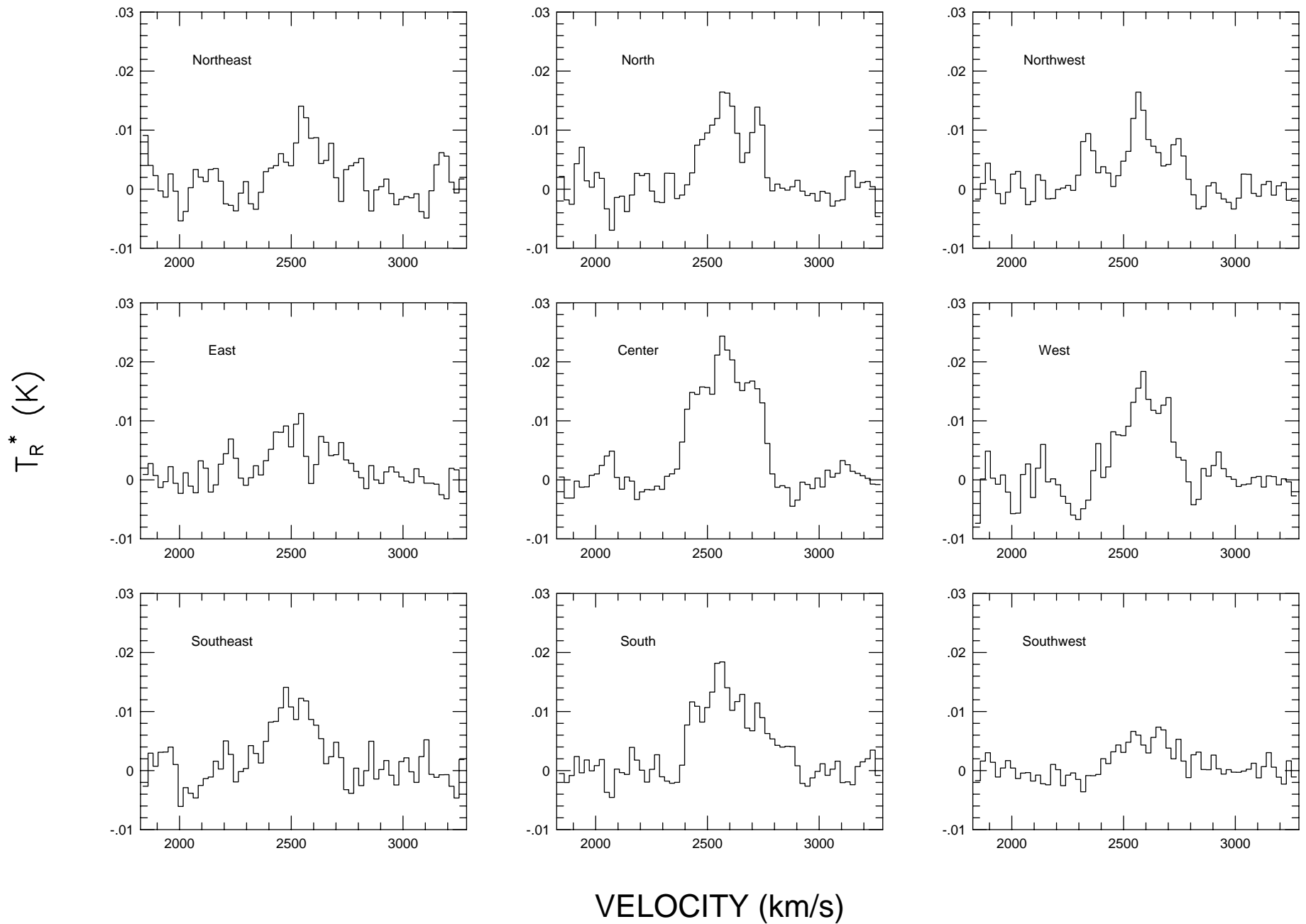
---

<sup>g</sup>For the NGC 4438 CO clump, the quoted  $L_{H\alpha}$  was determined from the Kenney et al. (1995)  $H\alpha+[N II]$  map, assuming  $L_{H\alpha} = 0.38(L_{H\alpha+[N II]})$ , as determined by optical spectroscopy (Kenney et al. 1995). Because this gas is shock-excited (Kenney et al. 1995), this luminosity is listed as an upper limit; it is an upper limit to the  $H\alpha$  luminosity due to young stars.

<sup>h</sup>For the NGC 4676 tail,  $L_{H\alpha}$  within the  $55''$  12m beam was determined from the Hibbard & van Gorkom (1996) map by Hibbard (1998, private communication), assuming  $L_{H\alpha} = 0.7(L_{H\alpha+[N II]})$ .  $M_{H_2}$  is from Smith & Higdon (1994).  $\Delta v/R$  and  $\sigma_v$  are from Hibbard & van Gorkom (1996) map as given by Hibbard (1998, private communication).

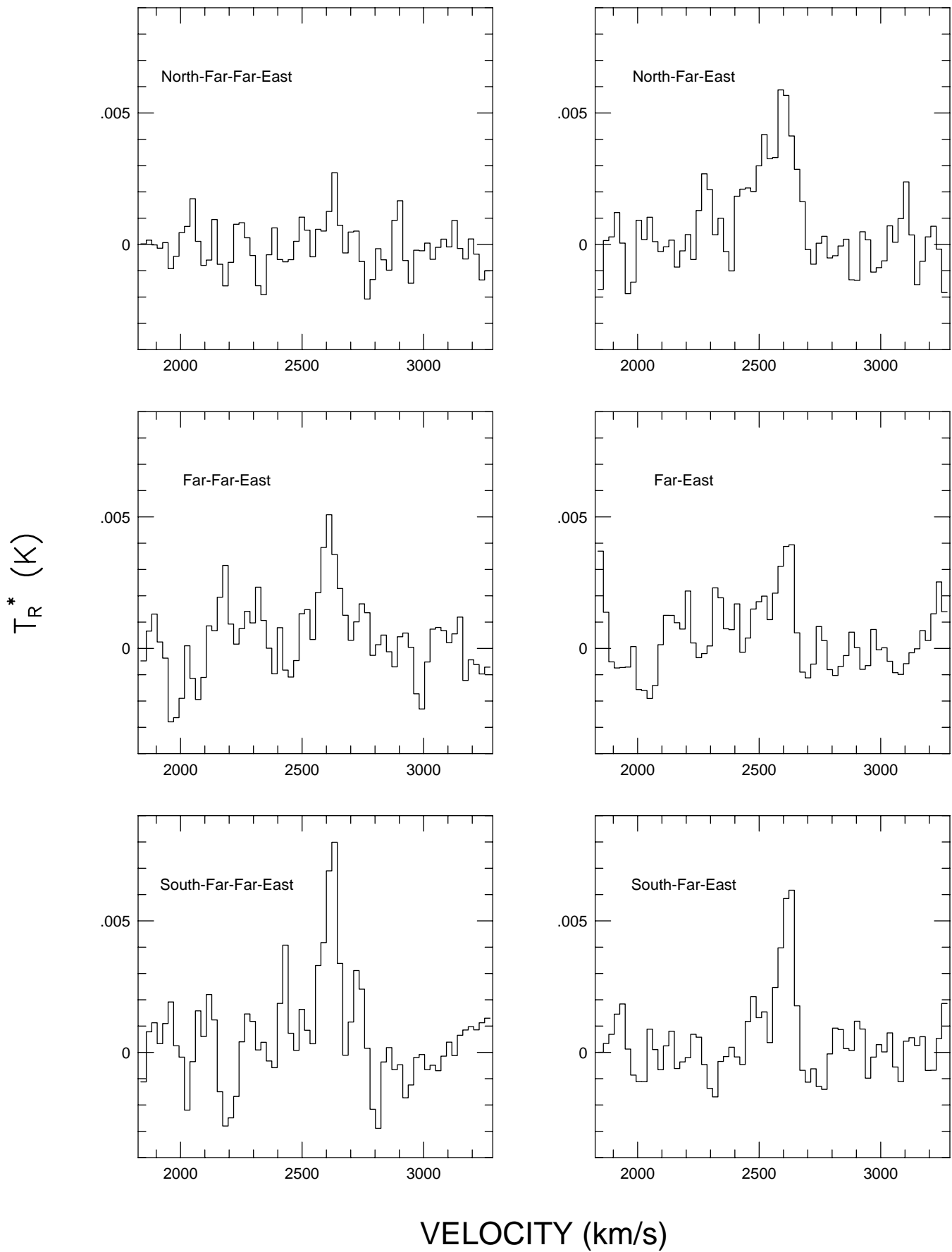


# NGC 2782 CO (1 - 0): THE MAIN DISK POSITIONS





# NGC 2782 CO (1 - 0): THE EASTERN TAIL



# NGC 2782 CO (1 - 0): THE WESTERN TAIL

